Q. J. R. Meteorol. Soc. (1999), **125**, pp. 2643–2661

A case-study of pronounced perturbations to cloud properties and boundary-layer dynamics due to aerosol emissions

By J. P. TAYLOR[1]* and A. S. ACKERMAN[2]
[1]*Meteorological Research Flight, Meteorological Office, UK*
[2]*University of Colorado, USA*

(Received 11 March 1998; revised 10 December 1998)

SUMMARY

During June 1994 the UK Meteorological Office C-130 aircraft took part in the Monterey Area Ship Tracks experiment. On 13 June 1994 a merchant vessel, the *Sanko Peace*, was observed steaming below a layer of broken stratus clouds in a shallow (300 m deep) boundary layer. These clean maritime clouds were significantly modified by the aerosol emissions from the ship. Droplet concentrations increased from around 10 cm^{-3} in the background cloud to a peak of 120 cm^{-3} in the ship track. This resulted in a roughly 50% reduction in average droplet size and drizzle flux. Less than an hour downwind of the *Sanko Peace*, the cloud top in the ship track was observed to be elevated by 100 m above the surrounding cloud tops.

A one-dimensional (1-D) model with size-resolved cloud microphysics, a detailed radiation code, and a turbulence closure scheme is used to simulate the observed ship track. The model predicts the observed microphysical changes reasonably well and also predicts a deepening of the boundary layer, though the simulated deepening is considerably slower than was observed. The driving force in the modelled response is an increased buoyancy flux due to enhanced radiative cooling in the cloud layer. The modelled boundary layer deepens in response to an increase in cloud water, which results from suppression of the drizzle flux. Differences between the modelled and observed profiles of cloud water in the ship track are difficult to reconcile with the modelled mechanism for the deepening, and are attributed to shortcoming in the 1-D model representation.

KEYWORDS: Aircraft measurements Boundary-layer dynamics Cloud radiative properties Ship tracks

1. INTRODUCTION

The effects of aerosols on clouds remain a major concern to climate modellers trying to predict the impact of anthropogenic aerosols on global climate. Squires and Twomey (1960) found that the droplet concentration in maritime clouds was lower than that observed in continental clouds due to the differing number of cloud condensation nuclei (CCN). Because cloud albedo depends on droplet concentration, and air pollution modifies CCN concentrations, Twomey (1974) suggested that pollution affects climate through the short-wave heat budget. In a recent assessment of climate change since pre-industrial times, the greatest uncertainty in any of the considered factors was attributed to this 'indirect' aerosol effect (Shine *et al.* 1995).

The ship-track phenomenon offers a unique way of studying the impact of anthropogenic aerosols on an otherwise unperturbed cloud field. In this study the term 'ship track' will be used to describe the region of the boundary-layer cloud field where the cloud microphysics is modified by the aerosol emissions from a ship exhaust.

Ship tracks were first observed in visible satellite imagery, under conditions ranging from apparently clear to overcast (Conover 1966). Conover recognized that the concentrations of CCN in a ship plume could overwhelm the background aerosols, whereas the vapour and heat from the ship exhaust would produce only negligible perturbations when mixed over a ship track kilometres wide. More commonly, ship tracks have been observed in near-infrared satellite imagery as bright linear features in marine stratocumulus fields (Coakley *et al.* 1987).

Radke *et al.* (1989) presented the first *in situ* measurements of ship tracks, which were obtained in an optically thick stratocumulus deck off the coast of southern California. They showed that the droplet size in the ship track decreased significantly and that

* Corresponding author: Remote Sensing Branch, Building Y70, DERA, Farnborough, Hampshire GU14 0LX, UK. e-mail: jptaylor@meto.gov.uk

the liquid water content in the ship track was significantly enhanced. To account for the enhancement of cloud water, Radke *et al.* invoked the hypothesis advanced by Albrecht (1989), in which an increase in droplet concentration leads to a decrease in droplet coalescence and a suppression of drizzle, thereby allowing cloud water to increase.

Long-wave radiative cooling near cloud top drives boundary-layer mixing in stratocumulus regions (Lilly 1968). Therefore, when droplet coalescence significantly reduces CCN concentrations (Hudson and Frisbie 1991; Akerman *et al.* 1994), allowing drizzle to deplete cloud water, long-wave absorption can diminish enough to allow the entire boundary layer to collapse to a shallow fog layer driven by surface mixing (Ackerman *et al.* 1993). An injection of CCN into such a collapsed boundary layer could then reverse the collapse, allowing the boundary layer to deepen as a persistent, optically thick cloud forms (Ackerman *et al.* 1995b).

During June 1994 the United Kingdom Meteorological Office (UKMO) Meteorological Research Flight (MRF) C-130 took part in the Monterey Area Ship Tracks (MAST) experiment. This multi-national experiment was aimed at looking at the ship-track phenomenon in the extensive stratocumulus off the west coast of the USA. In this paper, data from one flight of the MRF C130 during MAST is presented, in which a dramatic ship track was observed to deepen the boundary layer rapidly by 33%. Due to the presence of overlying cirrus clouds at the time of the satellite overpass, no satellite images of the track are available.

These measurements will then be used to initialize and evaluate one-dimensional (1-D) model simulations of the ship track. This 1-D model was developed to study aerosol–cloud interactions over long time-scales under horizontally homogeneous conditions, but the ship track in this case-study was observed to alter the boundary layer rapidly, in a decidedly horizontally inhomogeneous fashion. Our objective in comparing the model simulations is simply to gauge how well the 1-D model can reproduce these very interesting observations.

In section 2 a brief description of the key instrumentation used during MAST is presented, the aircraft observations are presented and discussed in section 3, and in section 4 the model simulations are presented.

2. Instrument description

The MRF operates a Royal Air Force C-130 Hercules aircraft that has been modified extensively to make it suited to a wide range of atmospheric research work.

A brief description of some of the instruments is given here. A more complete description of the standard meteorological instrumentation is given by Rogers *et al.* (1995), of the cloud physics instrumentation by Martin *et al.* (1994) and Brown (1993), and of the radiation instrumentation by Kilsby *et al.* (1992) and Saunders *et al.* (1992).

(*a*) *Radiation instrumentation*

Broad-band hemispherical irradiances are measured with Eppley pyranometers, two on the top of the aircraft and two on the underside. Each pair consists of one instrument fitted with a clear dome (Schott filter WG295, passband approx 0.3 to 3.0 μm) and another fitted with a red dome (Schott filter WG715, passband approx 0.7 to 3.0 μm). The red-dome filter separates the near-infrared part of the solar spectrum, where absorption by water vapour and condensed water are important, from the visible part, where molecular scattering is significant. The visible irradiance can therefore by computed by differencing the clear-dome and red-dome measurements.

Under conditions of predominantly direct irradiance the upper instruments have to be corrected for deviations from the local horizontal and a non-ideal cosine response. A thorough description of the techniques used is given by Saunders *et al.* (1992), whose results suggested that diffuse irradiances were the most accurate measurements, approaching 2%. For clear-sky downwelling irradiances the levelling and non-cosine corrections act to increase the uncertainty in the measurements to approx 3%.

A multi-channel radiometer (MCR) (Rawlins and Foot 1990) measures radiances in 14 narrow spectral bands between 0.55 and 12 μm. The MCR is mounted in a pod on the port wing of the aircraft and can view in the zenith, nadir and at angles out to 60° from the nadir. Internal calibration targets can also be viewed for calibration of the thermal infrared channels. The field of view of the optical system is 1.5°. The incident radiation is split into four streams, two thermal and two solar, and viewed by four detectors. Each detector has a rotating filter wheel with four filters. One complete revolution of a filter wheel takes four seconds.

Cloud optical depth, τ, and cloud droplet effective radius, r_e, can be retrieved using measurements of the reflectance at two wavelengths in the visible or near infrared. The reflectivity in a spectral region of weak liquid water absorption (e.g. 0.55 or 1.25 μm) is relatively insensitive to changes in r_e but monotonically increases with increasing τ; this allows a retrieval of τ by reference to a look-up table of model reflectances for varying clouds. This retrieved τ can then be combined with the reflectance at a wavelength of strong liquid-water absorption (e.g. 2.01 or 2.26 μm) to retrieve r_e. A thorough description of the scheme is given by Rawlins and Foot (1990) and an improvement to the scheme is given by Taylor (1992).

(*b*) *Aerosol and cloud physics instrumentation*

The cloud particle size distribution is measured by a Particle Measuring Systems (PMS) Forward Scattering Spectrometer Probe (FSSP). Particles are assumed to be perfectly spherical and composed of pure water. Measurements of the rate of sizing events and the true air speed allow inference of droplet number densities. The instrument records the number of droplets detected in 15 size categories in one of four ranges of droplet diameters selected by the operator: 2 to 47 μm, 2 to 32 μm, 1 to 16 μm or 0.5 to 8 μm. The first of these size ranges was selected for the measurements presented here.

The FSSP is calibrated by sampling glass beads of known sizes, allowances being made for the difference in refractive index of glass to that of water. The accuracy of the FSSP sizing is, at best, ± 1 μm radius.

The droplet spectra are used to compute r_e defined as:

$$r_e = \frac{\int n(r) r^3 \, \mathrm{d}r}{\int n(r) r^2 \, \mathrm{d}r} \tag{1}$$

where r is the droplet radius and $n(r)$ the concentration of droplets of radius between r and $r + \mathrm{d}r$.

Larger water droplets are measured using a PMS 2-DC probe. This instrument images particles in the range 25–800 μm diameter. In the 2-DC probe an array of photodiodes are illuminated by a He–Ne laser. A particle in the airflow will cross the laser beam and cast a shadow on the photodiodes. These images can be sized and counted to produce droplet size spectra. Combining the spectra from the FSSP and 2-DC instruments to give an r_e therefore includes the contribution due to the larger, drizzle-sized droplets. Equal weighting is applied to the FSSP and 2-DC data in their overlap region.

Aerosol concentration is measured by a PMS Passive Cavity Aerosol Spectrometer Probe (PCASP). This instrument counts and sizes aerosol in 15 size intervals covering the size range 0.1–3.0 μm diameter. Heaters in the tip of the inlet pipe to the PCASP and the sheath of dry air used to 'focus' the sample into the path of the laser beam both act to dry the aerosol. However, if the aerosol is particularly moist, or indeed saturated within cloud, then spurious results can be obtained. Also shattering of water droplets on the probe inlet can cause anomalously large concentrations to be recorded. For these reasons measurements made by the PCASP are used only out of cloud.

3. AIRBORNE OBSERVATIONS OF A SHIP TRACK

On 13 June 1994 the MRF C-130 flew a scientific sortie to study the impact of aerosol emissions from ships in the eastern Pacific off the coast of Monterey (35°N, 122°W) on the marine boundary-layer clouds predominant in that area. The times of data collection are quoted in GMT, Monterey local time is eight hours behind GMT.

The boundary layer on this day in the area of operation was characterized by a shallow stratus cloud deck with tops at around 300 m. This cloud layer was believed to extend to the ocean surface, although due to safety limitations the MRF C-130 was unable to profile below 150 m as the cloud extended below that altitude and the sea surface was not visible. Providing some corroboration, under similar conditions in the same region (very low CCN concentrations and a shallow boundary layer), cloud base was observed to extend to the surface (Hindman *et al.* 1995).

Soundings of temperature and water mixing ratios from a profile through the background clouds are shown in Fig. 1 from 1942 to 1948 GMT. Together with a roughly constant equivalent potential temperature (not shown), these profiles indicate a relatively well-mixed boundary layer around 300 m deep. The stratus had a banded structure which was clearly observed in the Modis Airborne Simulator imagery gathered during a flight of the NASA* ER-2 aircraft on the same day. A roll structure in the boundary layer was observed on several occasions during the MAST experiment and the turbulence structure associated with these features is described by Brooks and Rogers (1997). The wind in the boundary layer was strong at 9.4 m s^{-1} from the north-west. If one takes this wind, u, as being representative of the entire boundary layer then the depth of the boundary layer, d, that can be supported by the surface stress alone is given by the expression $d \sim 0.2u^*/f$, where f is the coriolis parameter, and the friction velocity u^* is determined from the approximate relation $u^* \sim u/28$ (Nicholls 1985). This term is often referred to as the surface mixed-layer depth-scale. In this case $d = 840$ m, the observed height of the subsidence inversion Z_i was at 300 m. Hence $d \gg Z_i$ which indicates that the surface stress alone was more than sufficient to maintain the depth of the boundary layer. (This analysis assumes neutral stability.)

The cloud was optically thin with a visible optical depth of around 5. This was retrieved by measuring the reflectance during a run above the cloud using the MCR (Taylor 1992). On the single occasion during the sortie when the MRF C-130 was able to profile to 15 m above the ocean surface in a cloudless area the boundary-layer aerosol concentrations were 10 cm^{-3}, identifying the region as a clean, unpolluted air mass.

During this sortie the C-130 was used to study a dramatic ship track formed by the merchant vessel *Sanko Peace*. A series of profiles through the cloud, and straight and level runs at various altitudes within and above the cloud, were flown. These measurements were flown so as to sample both the background cloud field and also

* National Aeronautics and Space Administration.

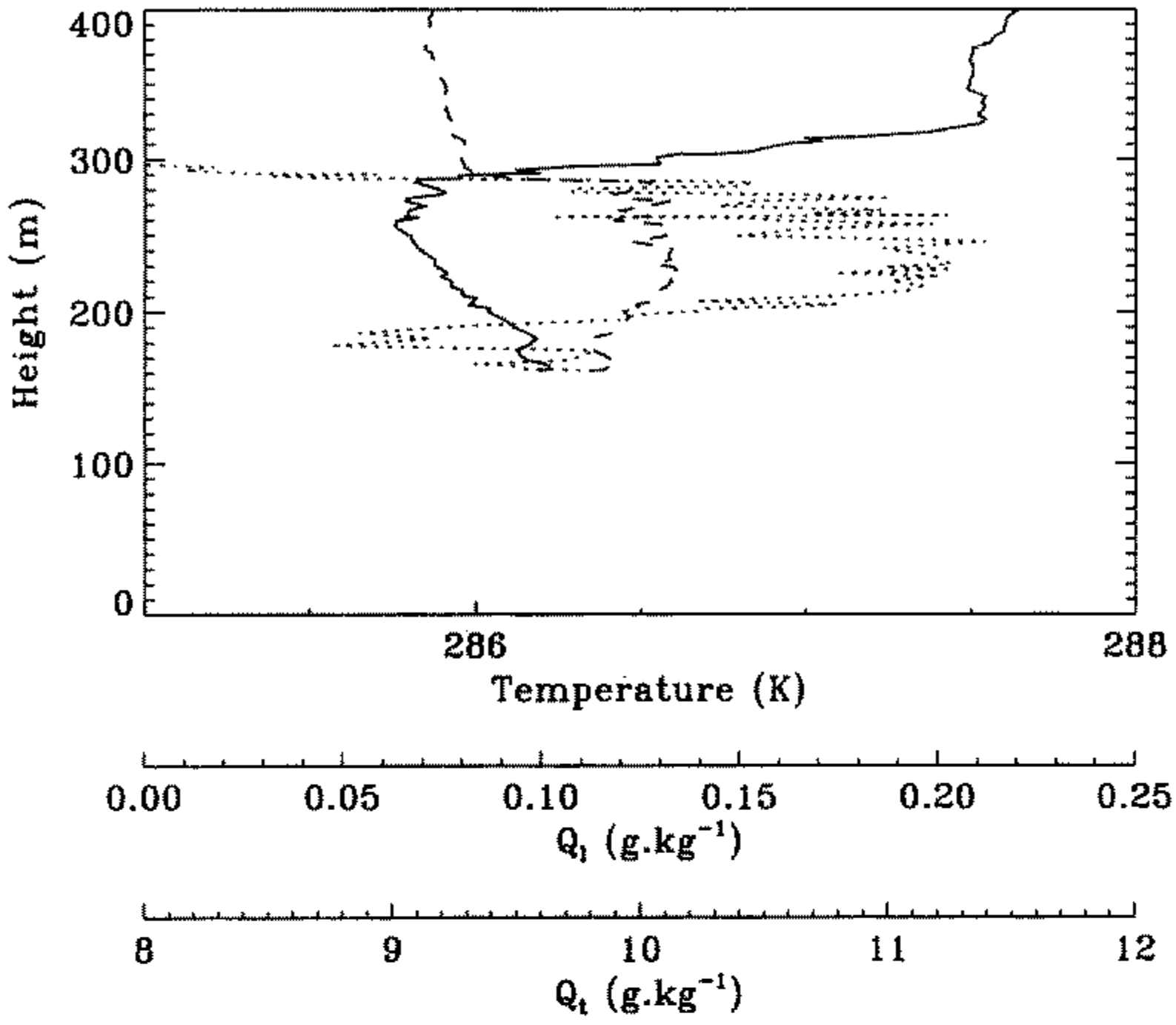

Figure 1. Profiles of temperature (solid line), total water mixing ratio, Q_t (dashed line), and liquid water mixing ratio Q_l, from the combined FSSP and 2-DC data (dotted line) measured during an aircraft sounding through the background clouds near the ship-track measurements from 1942 to 1948 GMT on 13 June 1994.

the cloud in the vicinity of the aerosol emissions from the ship. All the data presented here were gathered during flight legs perpendicular to the line of the ship track. The width of the ship track is therefore representative of the spreading of the exhaust plume.

In the background cloud the droplet concentration in the stratus was low. A run across the ship track was flown in cloud near the background cloud tops approximately 40 km from the ship (corresponding to about 35 minutes distance downwind, using the measured ship-relative wind speed of 20 m s^{-1}).

The measurements taken with the FSSP during this run are shown in Fig. 2. The droplet concentration, as measured by the FSSP, was observed to increase from a background value of between 5 cm^{-3} and 30 cm^{-3} to a peak value of 120 cm^{-3}. Large changes in r_e, as measured by the FSSP, were also observed. The average droplet concentrations (effective radii) were 12.0 cm^{-3} (14.2 μm) and 54.9 cm^{-3} (10.4 μm) in the background and ship-track clouds respectively, as measured by the FSSP. There were large amounts of drizzle-sized droplets which lie outside the sample range of the FSSP which were only seen by the 2-DC. Figure 3 shows droplet spectra measured using both optical probes during the ship-track transect previously shown. The background spectra are averaged over about 1 minute of flight before and 2 minutes after the ship track, and the ship-track spectra are averaged over a 30-second period within the track, as depicted in Fig. 2.

It is seen that mode radius decreased significantly and that the concentrations of drizzle-sized droplets also decreased as droplet concentrations increased in the ship track. The drizzle flux calculated for these spectra show that drizzle decreased from 0.9 mm d^{-1} in the background cloud to 0.5 mm d^{-1} in the ship track. The liquid-water content (LWC) was measured to decrease slightly, from 0.26 g m^{-3} in the background

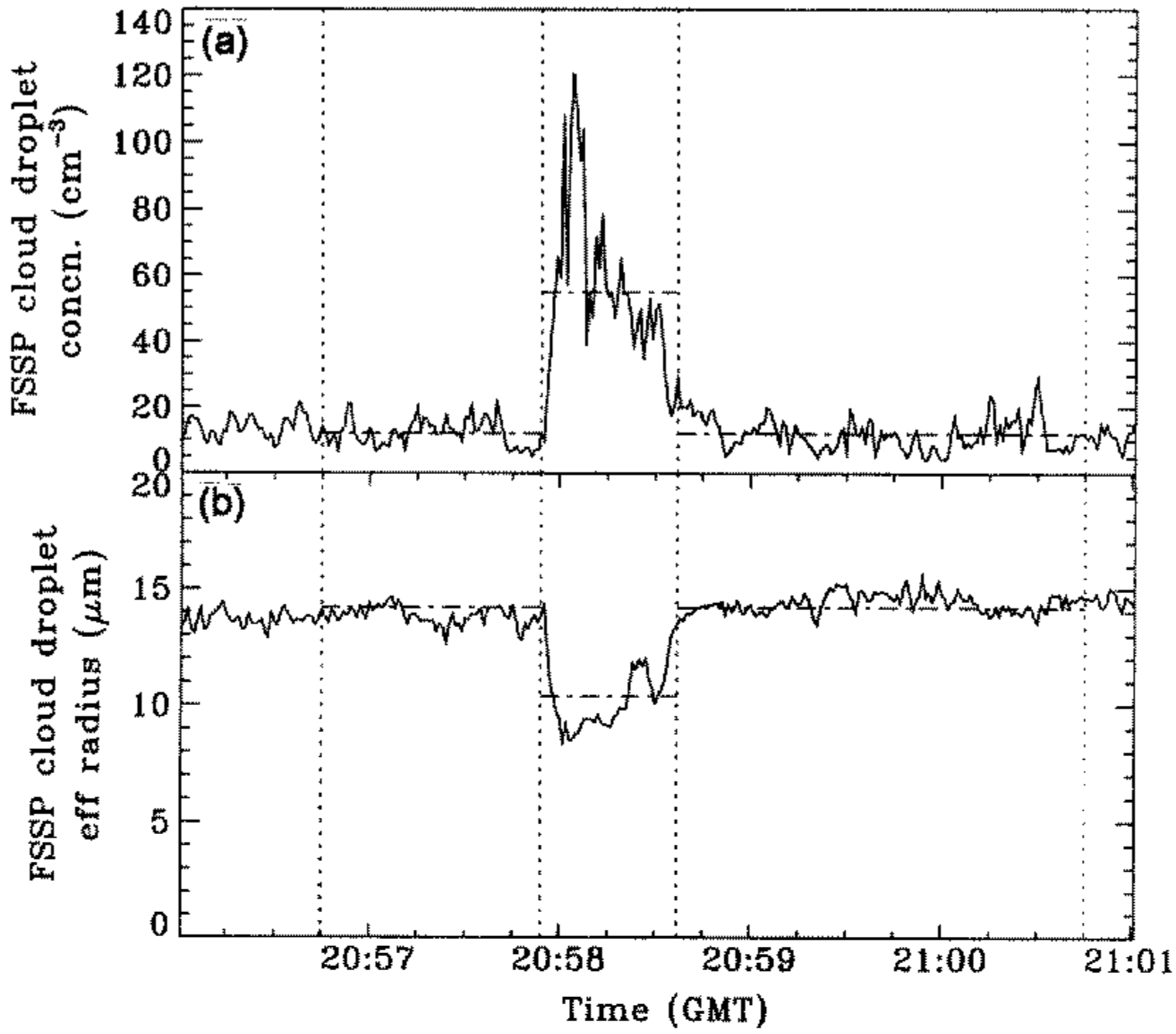

Figure 2. (a) Cloud droplet concentration and (b) cloud droplet effective radius measured by the FSSP on 13 June 1994 during a run across the ship track near cloud top, approximately 35 minutes in downwind distance from the ship. The vertical dotted lines denote the boundaries between the before-track, in-track and after-track time periods used when averaging the microphysical properties. The horizontal dashed lines denote the average cloud properties before, in, and after the ship track.

cloud to 0.24 g m^{-3} in the ship track. In contrast, a Johnson/Williams hot-wire probe, which is less sensitive to large, drizzle-sized droplets, measured a slight enhancement of LWC from 0.16 g m^{-3} in the background cloud to 0.18 g m^{-3} in the ship track.

After flying in cloud a run was flown above cloud and the reflectance of the cloud layer measured using the MCR. Figure 4(a) shows a retrieval of τ using the MCR at a wavelength of 1.25 μm during a run above cloud (data from 2042 to 2047 GMT) and Fig. 4(b) r_e measured in three different ways (data from 2057 to 2100 GMT). The dashed line is the FSSP r_e measured in cloud near the tops during the preceding run. The solid line with diamonds is r_e computed from the combined FSSP/2-DC spectra, taking 2-second averages. The solid line is the MCR retrieved r_e from the run above cloud using a combination of the reflectance data at 1.25 and 2.26 μm (Taylor 1992). In Fig. 4(a) τ was retrieved during a run above cloud ten minutes before the in-cloud run presented in Fig. 4(b). The co-location of these runs, to ensure that the same piece of the ship track was measured, was achieved by the aircraft navigator using the Global Positioning System and the average in-cloud wind speed to correct for drift of the cloud during the ten-minute interval between runs. This co-location was verified in the data processing by advecting the aircraft positions with the wind at the aircraft flight level and checking for consistency.

The combined FSSP/2-DC r_e is between 2 and 7 μm larger than that computed using the FSSP spectra alone in the background cloud. In the ship track the combined FSSP and 2-DC r_e drops by approximately 10 μm, a very significant change. It is interesting

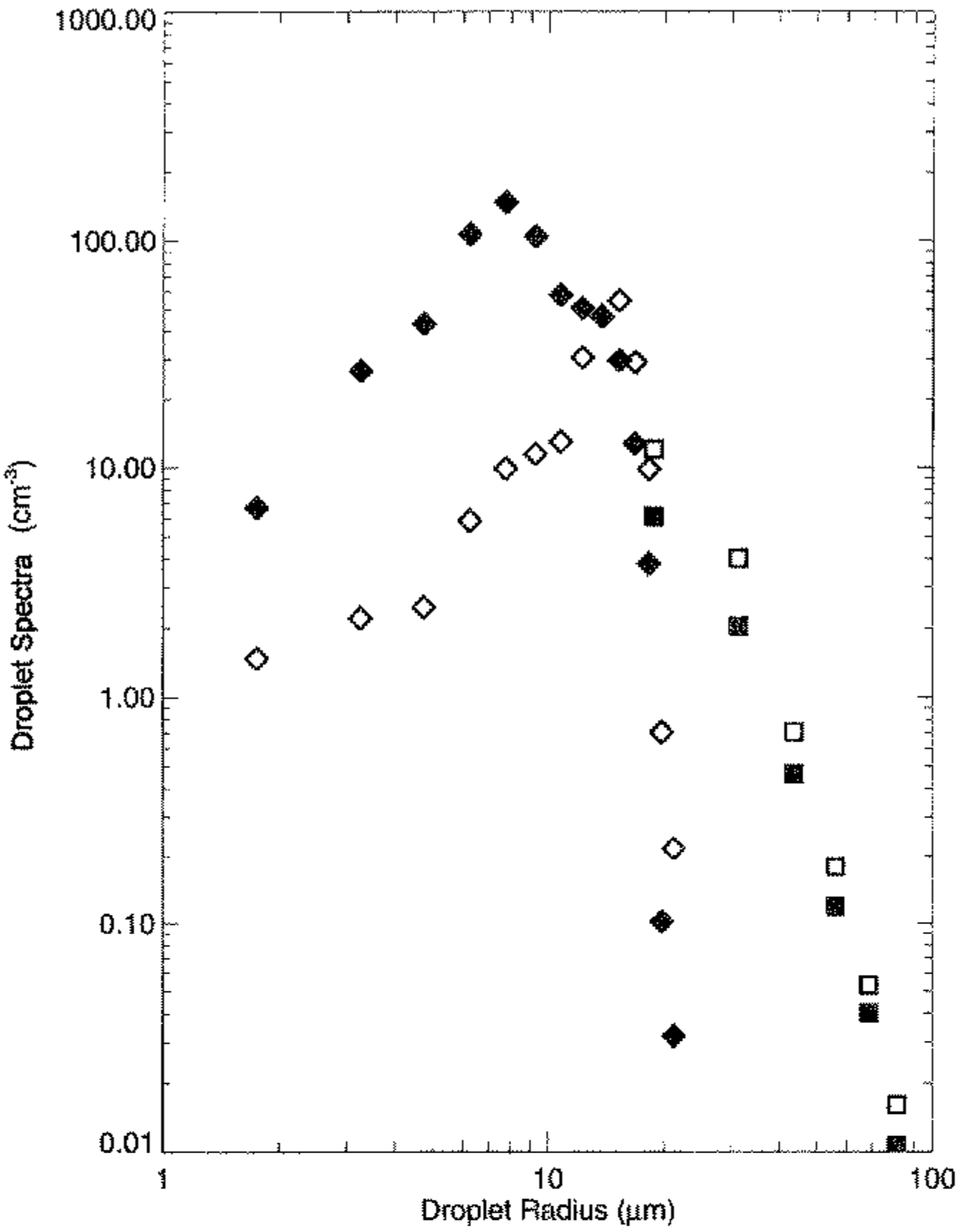

Figure 3. Combined FSSP (diamonds) and 2-DC probe (squares) droplet spectra from a run across the ship track near the height of the background cloud tops. The solid (open) symbols represent the averages from the ship track (background cloud) over the time periods indicated in Fig. 2.

to note that within the ship track the FSSP r_e and combined FSSP/2-DC r_e only differ by approximately 1 μm, further demonstrating that the increased droplet concentration has led to a suppression in the number of large, drizzle-sized droplets that are only observed by the 2-DC probe.

The MCR retrieval shows an increase in τ within the plume from a background value of around 5 to a peak value of 16. The MCR retrieved r_e is in very good agreement with that from the combined FSSP/2-DC and too shows a large decrease in r_e within the ship track. The retrieval results clearly show that this optical technique is sensitive to droplets both within the FSSP and 2-DC size ranges. Previous studies (e.g. Taylor 1993) have shown that the retrieved r_e is representative of the droplet spectra near the top of the cloud.

This large change in τ and r_e in the ship track modifies considerably the radiative properties of the cloud in the track. This ship track was visible to the naked eye as a band of increased brightness. Figure 5 shows the visible albedo (0.3–0.7 μm) measured during the run above cloud, and the cloud-top brightness temperature, as measured by the Barnes PRT-4 radiometer, during the same run. The visible albedo shows a 33% increase from a background cloud average of 0.33 to an average of 0.43 over the ship track. The peak albedo over the ship track was 0.51, representing a 54.5% increase. During this run above cloud it was observed that the top of the ship track was

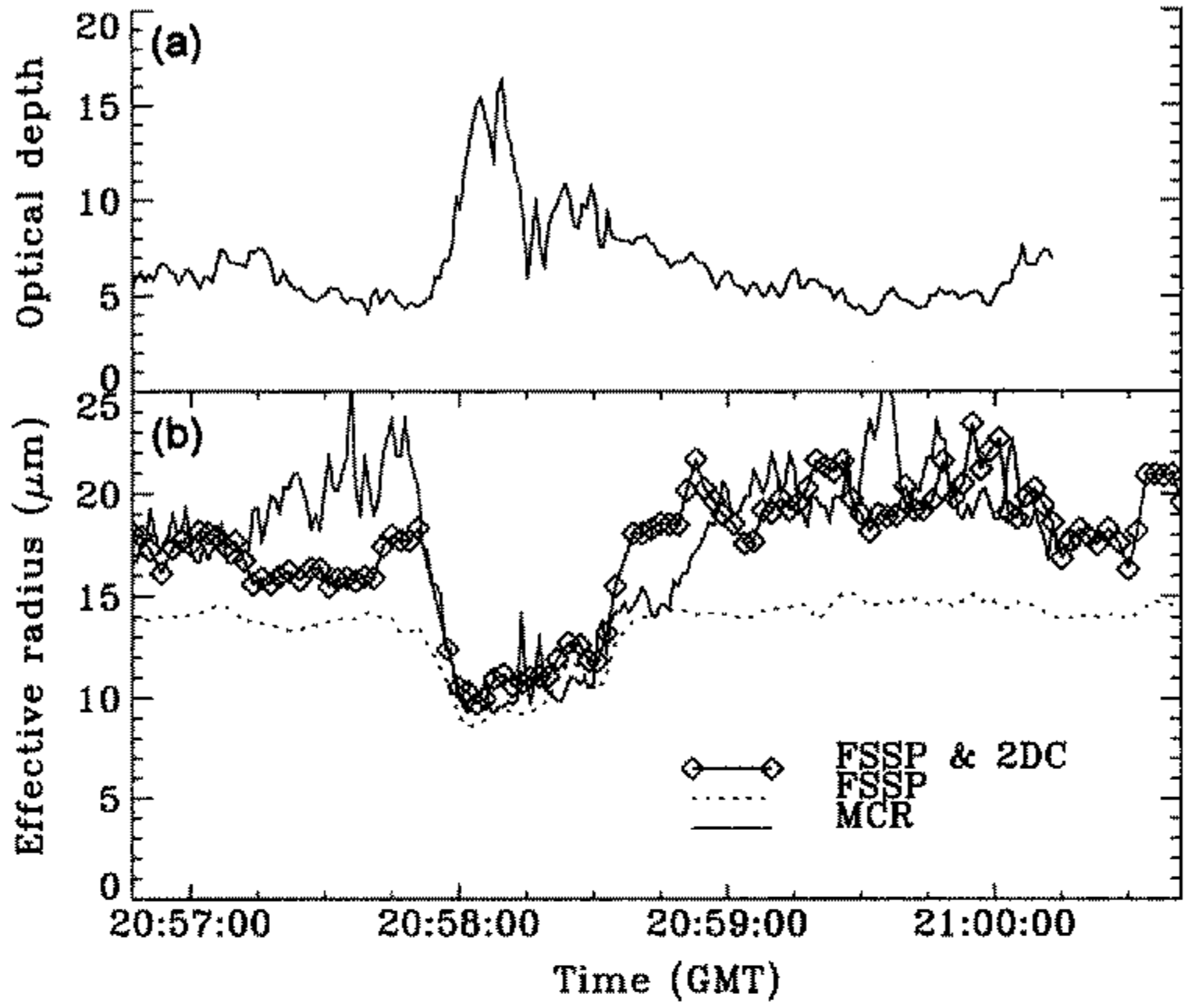

Figure 4. (a) Optical depth retrieved using the multi-channel radiometer (MCR) during a run above cloud crossing the ship track. (b) The effective radius measured during the previous run in cloud by the FSSP, the combined FSSP and 2-DC probes, and the retrieved effective radius using the MCR during the above cloud run. The times refer to the run in cloud on 13 June 1994.

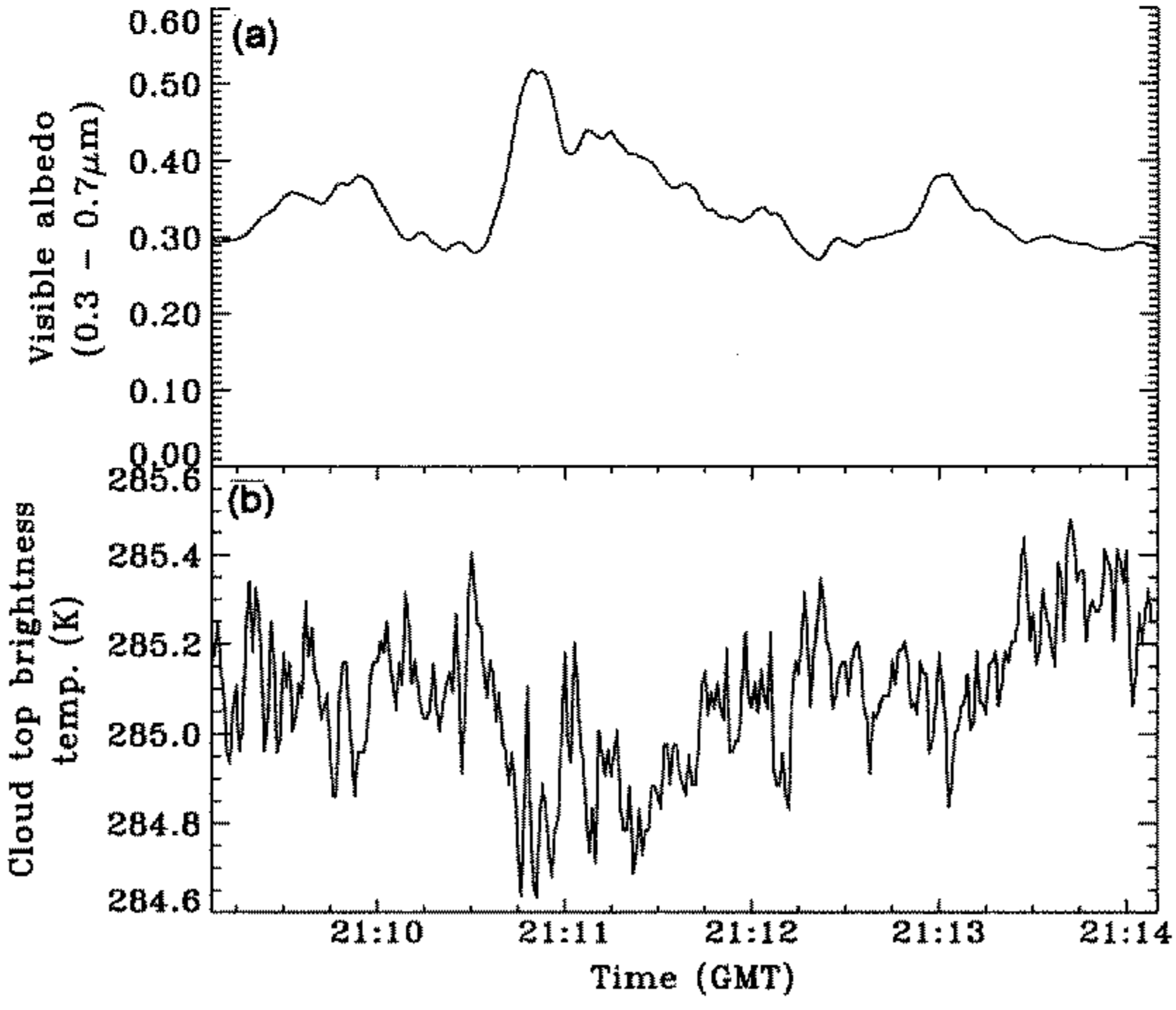

Figure 5. (a) The hemispherical visible albedo (0.3–0.7 μm) measured during a run above cloud crossing the ship track on 13 June 1994. (b) The cloud-top brightness temperature measured using a PRT-4 infrared radiometer.

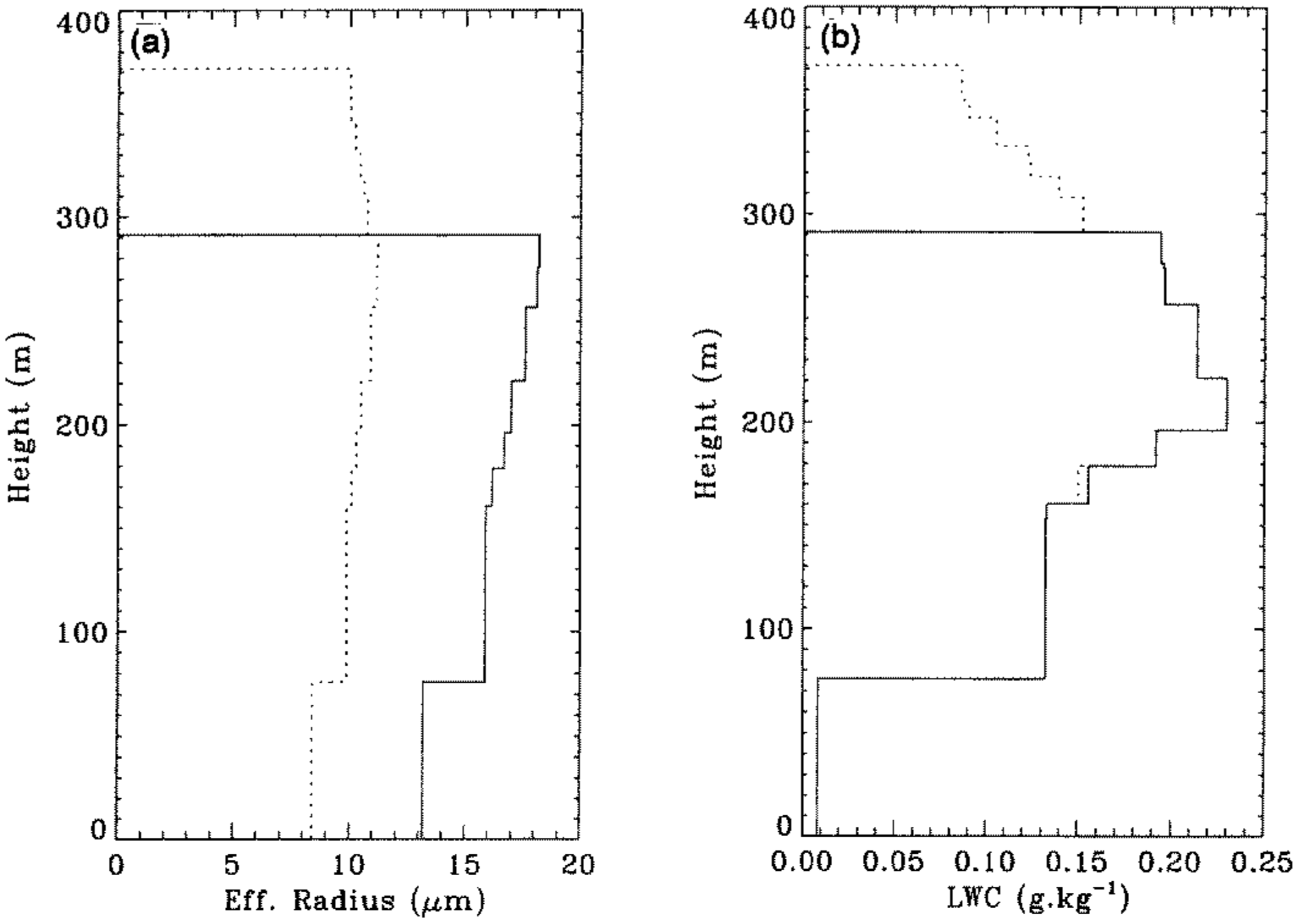

Figure 6. Profiles of (a) effective radius, and (b) liquid water content (LWC), used in the radiation modelling of the background cloud (solid line) and the ship track (dashed line). The vertical profiles were constructed from aircraft profiles through the cloud, and horizontal runs at various altitudes within the cloud layer.

elevated above the level of the background cloud. If one interprets the changes in the brightness temperature as being due to changes in cloud-top height then, using the in-cloud measured lapse rate of 4.0 K km^{-1}, the 0.4 K decrease in brightness temperature over the plume corresponds to an increase in cloud-top height of 100 m in the ship track. A level run flown 60 m above the background cloud intercepted the elevated ship track.

Profiles of the combined FSSP/2-DC r_e and LWC have been combined with measurements from straight and level runs to construct representative profiles of both the background cloud and the ship track (Fig. 6). For the following radiative calculations it has been assumed that the cloud reaches the sea surface, and in the ship track the top is elevated above that of the background cloud by 100 m. Both the background and ship-track cloud r_e increase linearly with height up to the height of the background-cloud tops. Above that r_e decreases with height in the ship track, indicating that rapid entrainment of free troposphere air was causing significant evaporation where the ship track was elevated above the surrounding clouds. In contrast, the background cloud was evidently entraining much slower (if at all). The liquid-water profiles are more complex. Both the straight and level runs and the profiles showed the maximum in liquid water to be in the middle of the cloud and that the LWC of the elevated plume was decreasing with height. The liquid-water paths of the two clouds, assuming they both extend to the surface, are 15 g m^{-2} for the background cloud and 69 g m^{-2} for the ship-track cloud.

These two profiles were used to compute the short-wave and long-wave heating rates using the radiation model of Edwards and Slingo (1996). This model has been extensively validated with aircraft observations by Taylor *et al.* (1996). The albedos

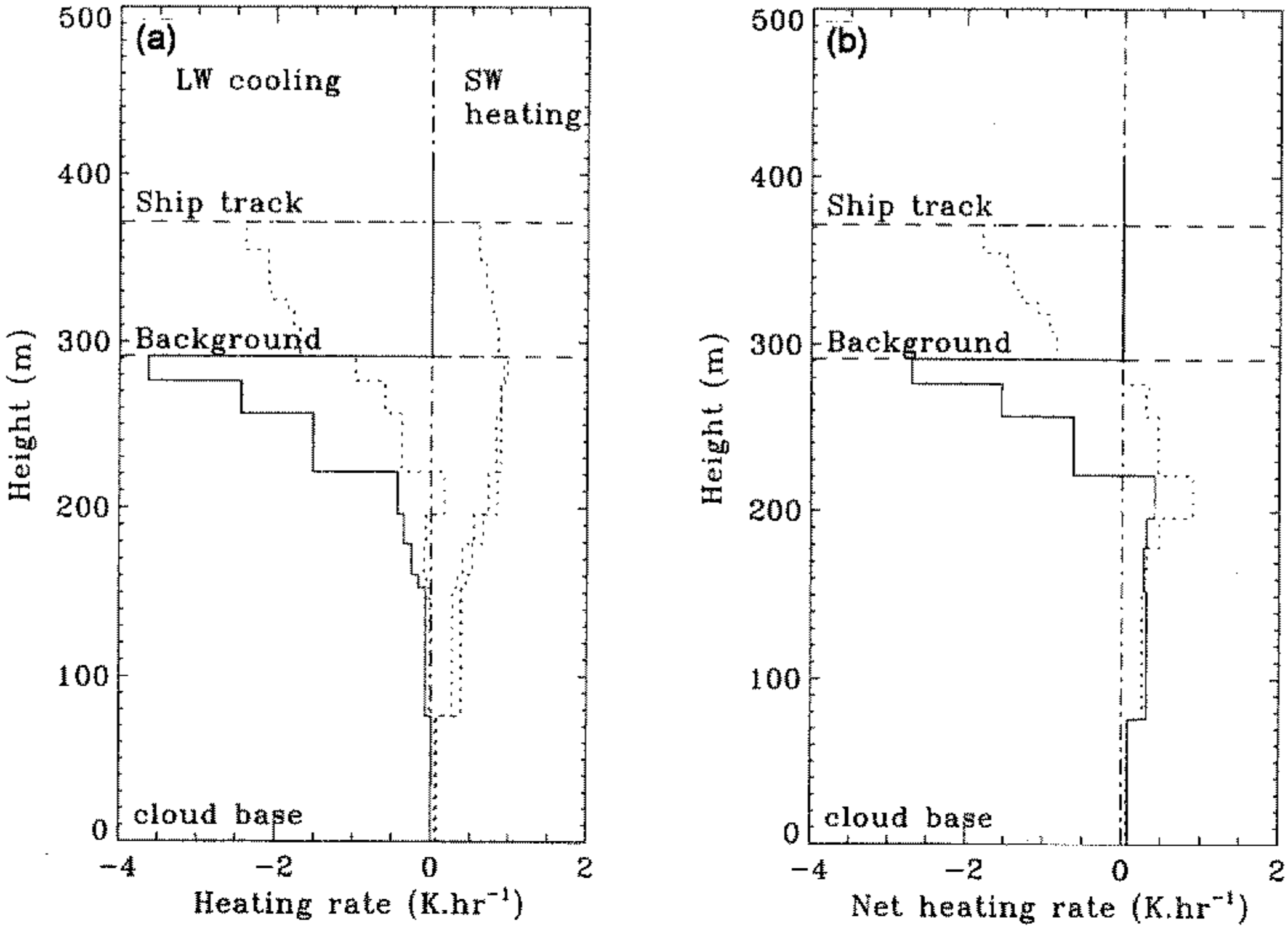

Figure 7. Results from the Edwards–Slingo radiation code for the two profiles shown in Fig. 6. (a) The heating rate for the long wave and short wave in both the background cloud (solid line) and the elevated ship track (dashed line) and (b) the net heating rate.

(0.3–0.7 μm) predicted by the model for the background and ship-track clouds were 0.23 and 0.45, respectively, which is in reasonable agreement with the observed increase from 0.33 to 0.43 (Fig. 5).

The results from the radiation model, at the observation solar zenith angle of 17°, are shown in Fig. 7. The model results show a very similar profile of heating within the cloud for both the ship track and the background cloud below the level of the background-cloud tops. The reduced liquid-water content in cloud tops in the ship track has resulted in a lower cloud-top long-wave cooling. The net effect on the heating rate is that the cooling at cloud top is slightly decreased in the ship track but the heating within the cloud is slightly increased.

4. Model simulation of ship track

In a previous modelling study, Ackerman *et al.* (1995b) predicted that, following the collapse of a cloud-topped marine boundary layer due to depletion of droplet concentrations (Ackerman *et al.* 1993), an injection of CCN could lead to an increase in boundary-layer depth. In their model results, a stratocumulus cloud layer can become so optically thin (at droplet concentrations below 10 cm^{-3}) that it can no longer drive boundary-layer mixing through cloud-top radiative cooling. They proposed that an injection of CCN into such a layer would lead to smaller droplets, which would coalesce less efficiently and result in a reduction of drizzle, thereby allowing cloud water to increase. The increased cloud water would then lead to a deepening of the boundary layer due to re-invigorated cloud-top radiative cooling. The conditions observed during

13 June suggested that the boundary layer had already collapsed: droplet concentrations were very low, the boundary layer was shallow, and the cloud layer may have reached the surface. Here we apply Ackerman *et al.*'s model to the ship track produced by the *Sanko Peace*.

The 1-D numerical model consists of three modules: a microphysics model that resolves explicitly the size distributions of aerosols and cloud droplets and treats the warm-cloud micro-physical processes that affect them, a detailed radiative-transfer model that calculates cloud optical properties and heating rates, and a turbulence kinetic energy (TKE) closure model that computes eddy-diffusion mixing coefficients (Ackerman *et al.* 1995a). Results of simulations with this model compare favourably with detailed observations (Nicholls 1984). The responses of the model to changes in boundary conditions (Ackerman *et al.* 1995a) and injections of CCN (Ackerman *et al.* 1995b) are also consistent with observations.

There are some fundamental shortcomings of this 1-D model. The model assumes horizontal homogeneous conditions and treats vertical transport through eddy diffusion. Such a treatment is most appropriate for stratus layers in which up draughts and down draughts do not maintain their identity through the depth of the cloud layer. Furthermore, only the mean supersaturation is represented at each grid level, which effectively assumes no covariance between supersaturation and the other microphysical fields (Stevens *et al.* 1998). As a result, peak supersaturations are averaged out, and the fraction of CCN activated to droplets is expected to be under-predicted by the model (Ackerman *et al.* 1995a). To get around this deficiency, the CCN concentrations used as input to the model are likely overestimated. Because of this short cut, we are simulating the response of the boundary layer to observed increases in droplet (rather than aerosol) concentrations.

Among the shortcomings of such a 1-D model is that by averaging over up and down draughts, peak supersaturations are averaged out, therefore the fraction of CCN activated to droplets is under-predicted by the model. To get around this deficiency, the CCN concentrations used as input to the model are artificially high.

Starting at local midnight, the background conditions were simulated for 12 hours using the observed boundary conditions as fixed values (with the exception of the solar zenith angle, which reaches 17° at noon). At noon, the simulation was split into two: in the control run the simulation was allowed to continue unperturbed for an additional 6 hours, while in the ship-track run a CCN injection (representing the ship exhaust) was instantaneously released at 100 m altitude, and this simulation also evolved for 6 hours. Because a 1-D model cannot represent horizontal dispersion, it is assumed that the CCN injection is immediately spread over a representative plume width.

The specified conditions for the simulations are based on measurements made during the aircraft profile at 1945 GMT (Fig. 1). The geostrophic winds were 12 m s^{-1} westward and 8.5 m s^{-1} northward (assumed to be independent of height). The sea surface temperature was set to 287 K, and the initial temperature profile followed a dry adiabat up to the base of the inversion (at 300 m), above which it linearly increased in a 200 m thick inversion layer to 292 K at the top of the model. The model domain was initially cloud free, with a relative humidity of 98.3% in the boundary layer and a water vapour mixing ratio of 9 g kg^{-1} above. The large-scale divergence was set to 5×10^{-6} s^{-1}, resulting in a subsidence rate of 0.15 cm s^{-1} at the top of the boundary layer. The water vapour column above the model domain was set to 5 g cm^{-2}, resulting in a downwelling long-wave flux near cloud top of 300 W m^{-2}, in agreement with the measurements. The initial distribution of (dry) particles was independent of altitude with

a concentration of 50 cm^{-3}, specified as a log–normal distribution (with a geometric mean radius of 0.08 μm and a geometric standard deviation of 1.3) of ammonium bisulphate, based on background measurements of accumulation-mode aerosols from the University of Washington (UW) C-131A on 27 June (Hobbs *et al.* 1999). Aerosol particles were created in the boundary layer at a rate of 1.7×10^{-3} $cm^{-3}s^{-1}$ (using the same distribution as in the initialization) throughout the simulation to offset losses due to aggregation and surface deposition. A crude parametrization is used for the aerosol source to bypass the complications of explicitly modelling the possible sources, which include surface sources of sea salt and possibly organics, photo-oxidation of gaseous precursors (and subsequent coagulation), and transport of pollution from distant sources (and subsequent entrainment). Because we constrain the model simulations to match the measured droplet concentrations, the overestimated initial aerosol concentration and the crudely parametrized aerosol source are simply short cuts for matching those constraints.

For the particle injection at noon in the ship-track run we used a log–normal distribution of ammonium bisulphate particles with a geometric mean radius of 0.045 μm and a geometric standard deviation of 2.7. The size distribution was taken from measurements made from the UW C-131A in the exhaust plume of the ship *Cosco Tai He* on 27 June (Hobbs *et al.* 1999). The particle injection strength was 3×10^7 cm^{-2}, which is a perturbation in particle concentration of 100 cm^{-3} averaged over the depth of the boundary layer. Using the measured ship-relative wind speed of 20 m s^{-1} and a plume width of 5 km, this injection requires a source strength of 3×10^{16} s^{-1}, which exceeds by a factor of 2 the source strengths estimated by Hobbs *et al.* (1999). The enhanced source strength was imposed to compensate for the likely under activation of CCN by the model (due to under-predicted peak supersaturations).

The results of the ship-track simulation are summarized in the time–height contour plots of cloud properties shown in Fig. 8. Early in the simulation cloud formation shocks the model and results in maxima of droplet concentrations, cloud water, and drizzle. The cloud layer thins slightly during the day as the model recovers from cloud formation and as the cloud layer absorbs solar energy (which offsets the slight buoyancy flux driven by infrared cooling). The injection of CCN at noon result in a drastic increase in droplet concentration (Fig. 8(a)), which leads to a reduction in the drizzle fluxes (Fig. 8(b)). The reduced precipitation sink allows the cloud water to increase (Fig. 8(c)), and also results in the increased mixing that deepens the boundary layer.

Comparison of the model results at a single altitude (200 m) with the observations is shown in Fig. 9. The model-simulated droplet concentration peaks at 0100 h due to the shock of cloud formation, after which it relaxes to a steady value of ~20 cm^{-3}, which is comparable with the measured background concentrations of 5 to 30 cm^{-3} (Fig. 9(a)). The modelled droplet r_e reaches a steady value of ~9 μm. The liquid-water path in the model results is 48 g m^{-2} at noon (Fig. 9(c)), in agreement with the radiometrically measured value of 41 g m^{-2} and also consistent with the general agreement between the measured and modelled profiles of liquid water (Fig. 10(a)).

Particles are injected into the ship-track run at noon and mix upwards to the cloud layer where the droplet concentrations rapidly increase to ~90 cm^{-3}, which exceeded the average concentrations of ~70 cm^{-3} measured near the head of the ship track (Fig. 9(a)), but was surpassed by the measured peak concentrations of 120 cm^{-3}. The droplet concentrations measured in the ship track diminished much more rapidly with time than in the measurements, due to the lack of horizontal dispersion in the 1-D model. The droplet effective radius in the ship track at 1300 h nearly matches

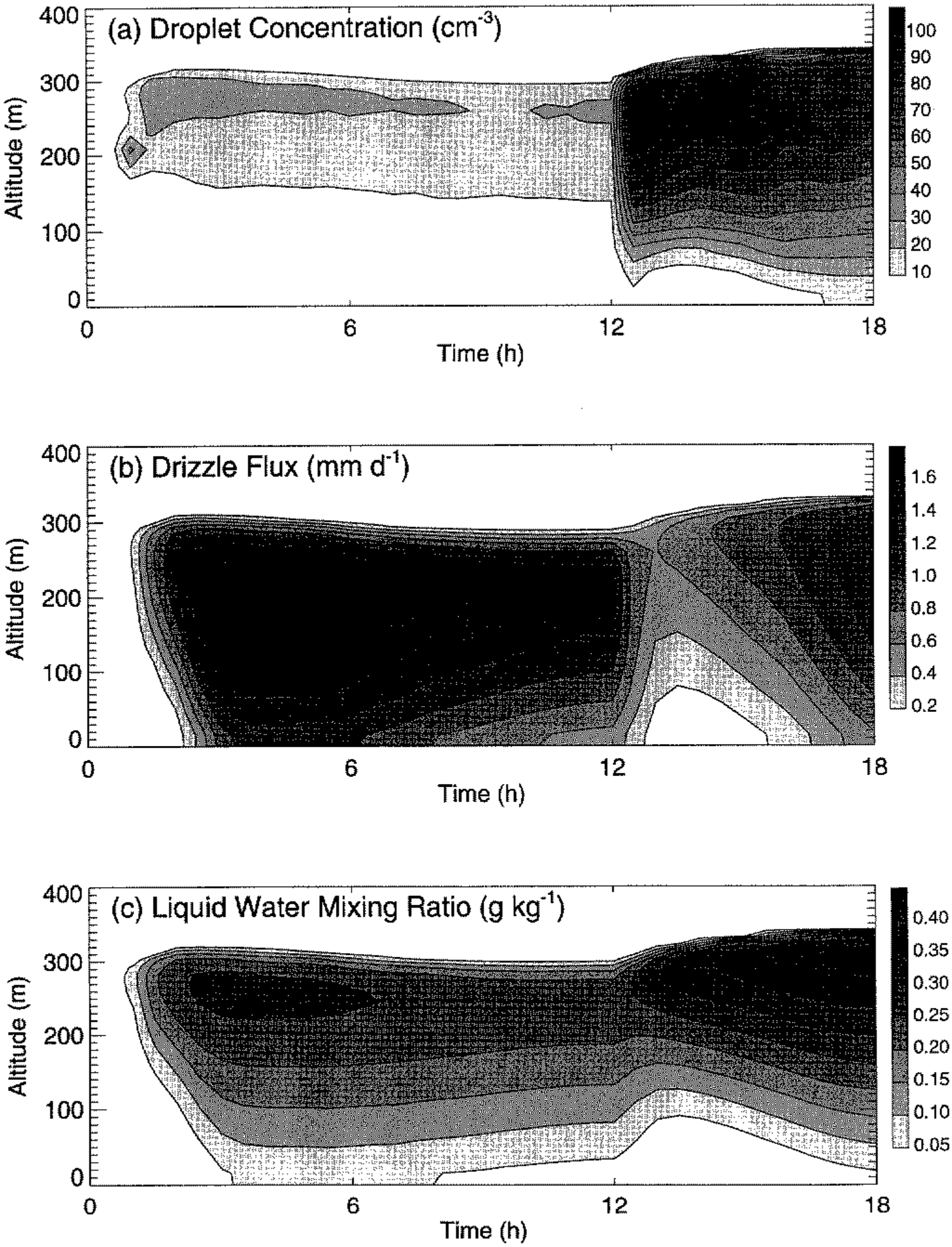

Figure 8. Time–height contours of (a) droplet concentration, (b) drizzle flux and (c) liquid-water mixing ratio in the ship-track simulation.

the measured average value of 10.4 μm (Fig. 9(b)). The significant change in droplet size resulted in an 80% relative increase in the modelled albedo above cloud top, from 0.22 in the control run to 0.39 in the ship-track run, in reasonable agreement with the observed increase from 0.33 to 0.43 near the head of the ship track. Because the smaller droplets are less efficient at producing drizzle (Fig. 10(b)), the modelled liquid-water path increases (Fig. 10(c)). The increase in the modelled cloud water near cloud top

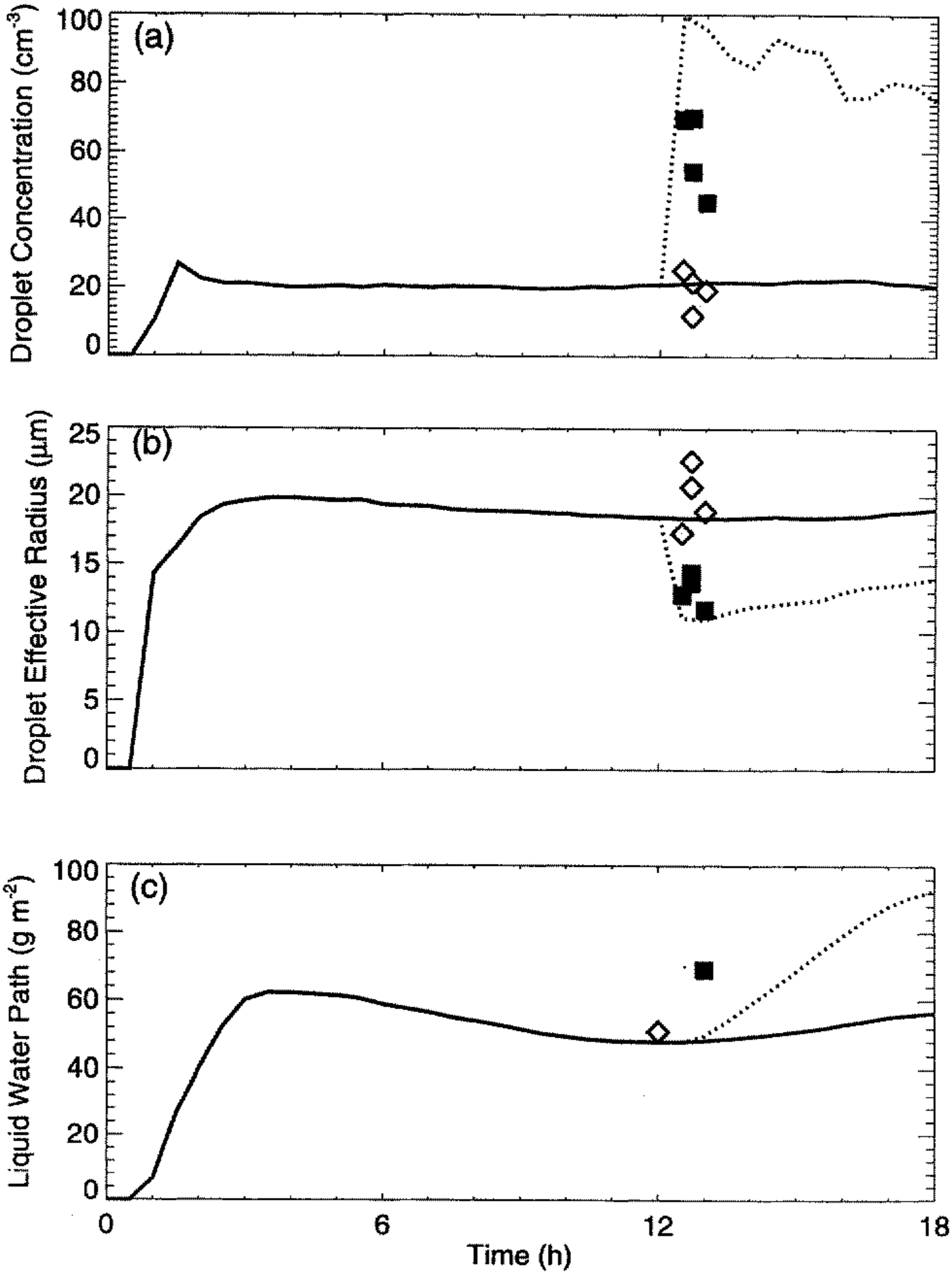

Figure 9. Time evolution of (a) droplet concentration, (b), droplet effective radius, and (c) liquid-water path. The solid lines are for the control run (background cloud) and the dotted lines are for the ship-track simulation. The model output in (a) and (b) are at 270 m altitude. Measurements (which are each averaged over kilometres of the C-130 flight path) of background values (diamonds) and from transects through the *Sanko Peace* ship track (squares) are shown for (a) and (b), where the head of the ship track is at 12 h. Radiometrically determined values from the C-130 above the cloud layer are shown for (c).

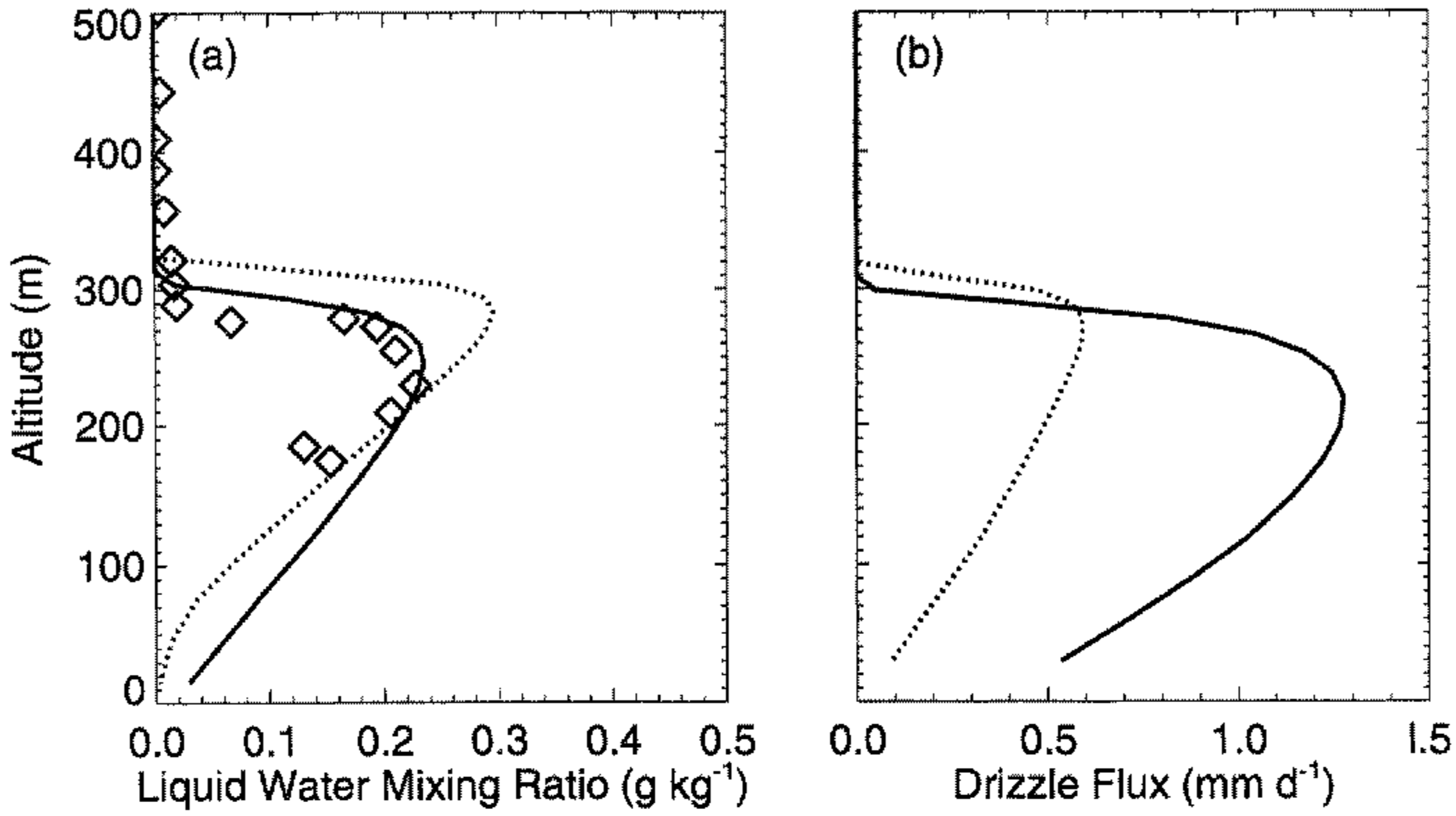

Figure 10. Model simulations at 13 hours of (a) liquid-water mixing ratio and (b) drizzle flux. The solid lines are for the control run (background cloud) and the dotted lines are for the ship-track simulation. The profile of liquid-water measured by the C-130 at 1945 GMT (using the Johnson/Williams liquid-water probe) in the background cloud is overlaid with diamonds in (a).

leads to increased solar absorption. However, the increased gradient in cloud water at cloud top also leads to increased long-wave cooling, which overwhelms the change in solar heating and results in an increase in net cooling (Fig. 11(a)). This increase in cloud-top cooling enhances the buoyancy flux (Fig. 11(b)), leading to an increase in turbulent mixing at cloud top that allows the boundary layer to deepen against the subsiding inversion air. In Fig. 10 it is seen that the boundary layer deepens by 20 m in one hour. The deepening continues for another two hours, when the boundary layer in the ship-track run is 50 m deeper than in the control run. Although this deepening in the model simulation resembles the observed behaviour, the deepening was greater and more rapid in the observed ship track, where the boundary layer deepened by ~100 m in less than one hour of evolution.

In both the ship-track run and the control cases the TKE budget is dominated by the shear term in the first hour after the aerosol injection was introduced. Figure 12 shows the heating rate five hours later. By this time the differences are more pronounced. The increase in cloud water has led to a significant increase in radiative cooling, so much that buoyancy has become the greatest source of TKE in the middle of the (ship track) cloud layer.

In this model simulation the initial cloud field was embedded in a collapsed boundary layer where, due to the low amounts of liquid water, the radiative cooling could not maintain the boundary-layer mixing. An aerosol perturbation has been introduced to simulate the effect of ship exhaust emissions. This aerosol has led to an increase in droplet concentration, a reduction in drop size, and an accompanying decrease in drizzle flux. The increased cloud-top long-wave cooling has been sufficient to increase the buoyancy within the cloud and elevate the ship-track cloud top to 50 m above that of the background clouds.

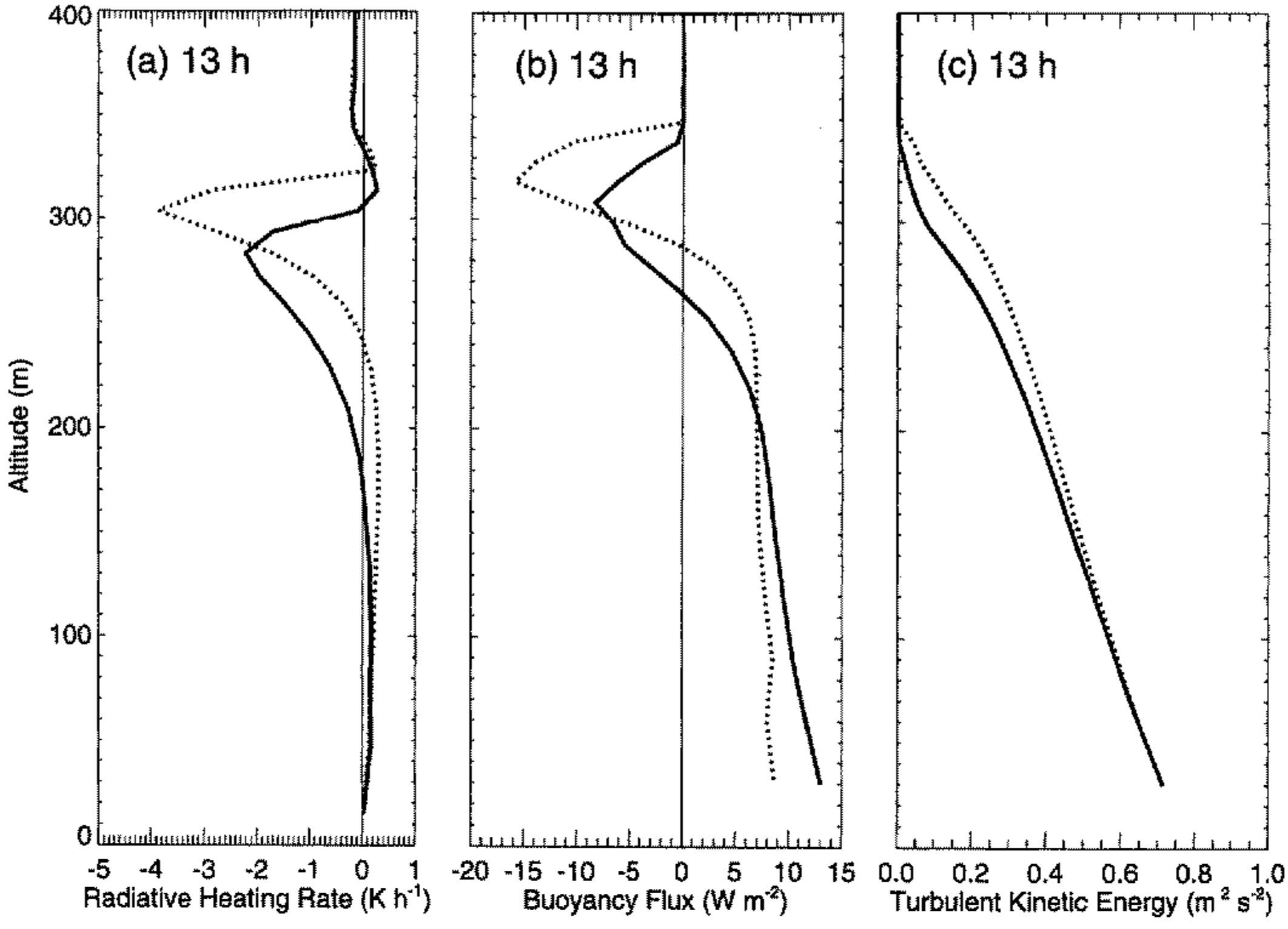

Figure 11. Model simulations at 13 hours of (a) net radiative heating rate, (b) buoyancy flux, and (c) turbulent kinetic energy. The solid lines are for the control run (background cloud) and the dotted lines are for the ship-track simulation. Model layers are 10 m thick in the cloud layer.

The response of the model at first glance seems to explain the deepening of the boundary layer in the observed ship track, though the magnitude and timing are under-predicted. However, the modelled mechanism requires a steepening of the gradient in liquid water near cloud top. Although no profiles were flown through the ship track, a profile composited from several horizontal flight legs showed a gradual decrease of liquid water near cloud top in the ship track, presumably due to evaporation where the cloud was entraining inversion air. It is not clear what to make of this apparent discrepancy, as the horizontal and temporal averaging performed for the composited profile are not directly comparable with the horizontal averaging implicit in the 1-D model framework. The slower deepening of the simulated boundary layer more directly points to another known problem with the 1-D model: simulations of collapsing boundary layers with a 3-D model indicate that the 1-D model does not adequately represent cumuliform convection (Ackerman *et al.* 1998). Hence, the 1-D model is not well-suited to simulating interactions between microphysics and convection over short time-scales, consistent with simulated boundary-layer deepening that is slower than was observed.

One could conceivably run sensitivity tests to evaluate the robustness of the model response. However, given the lack of a corroboration of the simulated response time, and the ambiguity of the comparison between the model results and the observation, there is little motivation for such an exercise. Furthermore, there are no compelling input parameters to adjust. The only unmeasured parameters of significance are the CCN activation spectrum and the large-scale divergence rate. Although there are a number of degrees of freedom in specifying the input CCN spectrum, these are ultimately constrained by

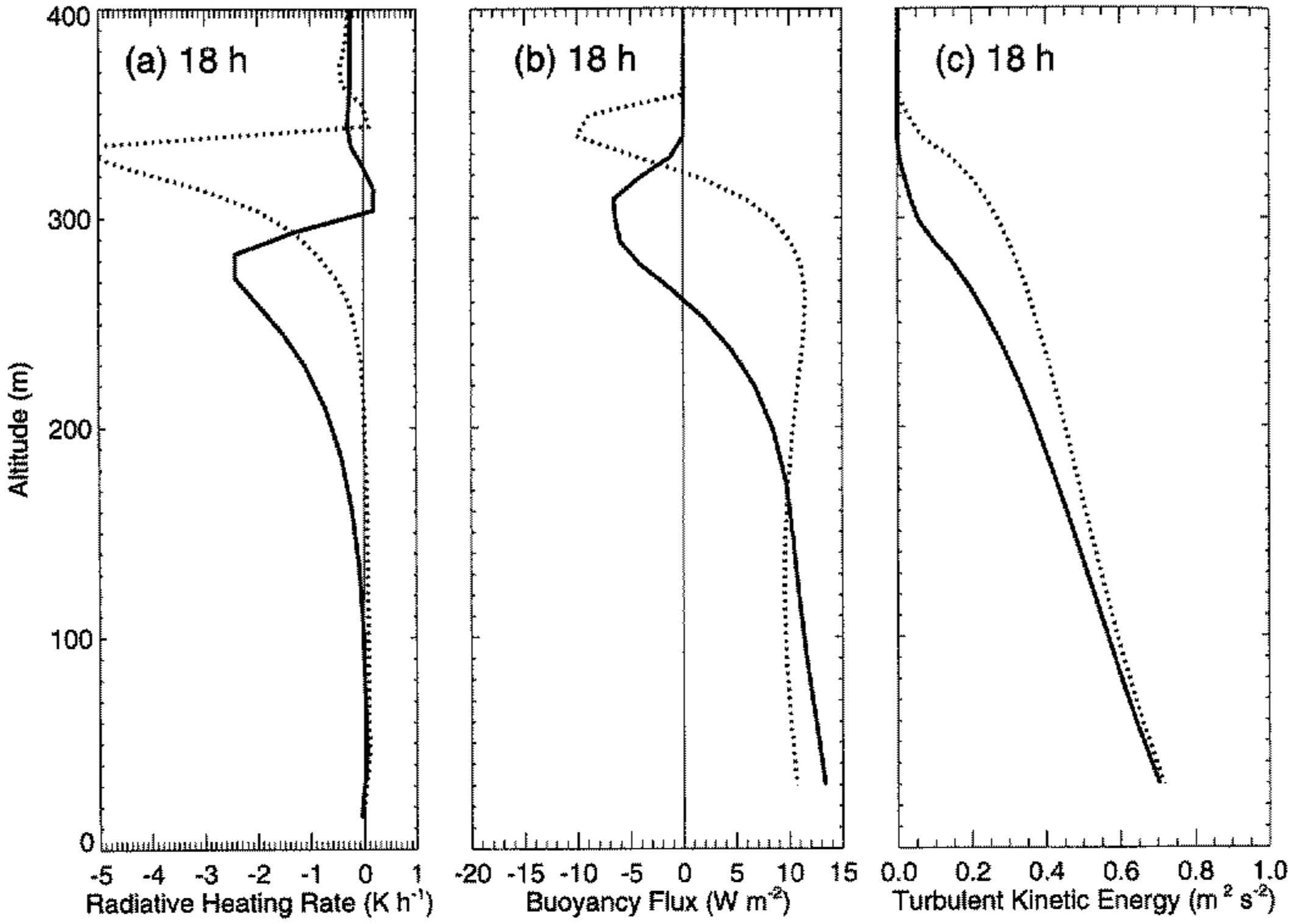

Figure 12. As Fig. 11 but for model simulations at 18 hours.

the measured droplet concentrations. The divergence rate was constrained by running the control simulation to determine what divergence reproduces the observed boundary-layer depth. Hence, all the input parameters are effectively constrained in a coupled sense by the observations.

5. Conclusions

The merchant vessel *Sanko Peace* was emitting aerosols that had a dramatic impact on the microphysics and radiative properties of a stratocumulus layer off the coast of California. This effect was enhanced by the very low droplet concentrations of the background cloud, leading to a high susceptibility to change in droplet number. Furthermore, as the background conditions were consistent with those of a collapsed boundary layer the increase in cloud droplets may have led to increased buoyancy forcing enough to deepen the boundary layer in the ship track.

The 1-D modelling results have described a possible mechanism for the changes observed. However, the 1-D model was unable to simulate the apparent decrease in cloud liquid water with height within the elevated ship track, and hence one cannot resolve completely the complex series of events that led to the elevated plume. Simulations with a 3-D model are required to resolve the motions involved in the entrainment of inversion air and the deepening of the boundary layer.

Anthropogenic aerosol emissions likely to be of climatic significance will occur over length-scales greater than those observed in the ship-track case presented here. Also, these emissions will affect the entire cloud evolution as opposed to being emitted into an otherwise clean cloud layer. Despite these differences in scale, the effects of

aerosols on clouds observed by ship tracks give us an indication of the processes that may be significant, and act as a good test bed of numerical models for simulating larger scale changes. These results have shown that the changes in droplet concentration, associated with increased CCN, not only reduce the droplet size but can also reduce the drizzle flux. The reduction in drizzle allows cloud water to increase, increasing cloud albedo. A realistic treatment of such feedbacks between cloud microphysical processes and macrophysical properties presents a formidable challenge to large-scale models. These observations suggest that reliable predictions of marine stratiform cloudiness may require predictions of aerosol concentrations.

Acknowledgements

We would like to thank the MRF scientists (particularly the flight scientist, Doug Johnson) and Royal Air Force aircrew of the MRF C-130 for their efforts in obtaining the data used in this paper. The coordination of the MAST experiment was carried out by Phil Durkee and Bob Bluth and their contributions are greatly appreciated. A. Ackerman was funded under NASA Grant NA65-6504 EOS Interdisciplinary Science.

References

Ackerman, A. S., Toon, O. B. and Hobbs, P. V. 1993 Dissipation of marine stratiform clouds and collapse of the marine boundary layer due to depletion of cloud condensation nuclei by clouds. *Science*, **262,** 226–229

1994 Reassessing the dependence of cloud condensation nucleus concentration on formation rate. *Nature*, **367,** 445–447

1995a A model for particle microphysics, turbulent mixing, and radiative transfer in the stratocumulus-topped marine boundary layer and comparisons with observations. *J. Atmos. Sci.*, **52,** 1204–1236

1995b Numerical modeling of ship tracks produced by injections of cloud condensation nuclei into marine stratiform clouds. *J. Geophys. Res.*, **100,** 7121–7133

Ackerman, A. S., Toon, O. B. and Stevens, D. E. 1998 'Response of the cloud-topped marine boundary layer to depletion of aerosol concentrations'. Pp. 322–324 in Conference on cloud physics, Everett, Washington, USA, 17–21 August 1998. American Meteorological Society

Albrecht, B. A. 1989 Aerosols, cloud microphysics and fractional cloudiness. *Science*, **245,** 1227–1230

Brooks, I. M. and Rogers, D. P. 1997 Aircraft observations of boundary layer rolls off the coast of California. *J. Atmos. Sci.*, **54,** 1834–1849

Brown, P. R. A. 1993 Measurements of the ice water content in cirrus using an evaporative technique. *J. Atmos. Oceanic Technol.*, **10,** 579–590

Coakley, J. A., Bernstein, R. L. and Durkee, P. A. 1987 Effect of ship track effluents on cloud reflectivity. *Science*, **237,** 1020–1022

Conover, J. H. 1966 Anomalous cloud lines. *J. Atmos. Sci.*, **23,** 778–785

Edwards, J. M. and Slingo, A. 1996 Studies with a flexible new radiation code. I: Choosing a configuration for a large-scale model. *Q. J. R. Meteorol. Soc.*, **122,** 689–719

Hindman, E. E., Porch, W. M., Hudson, J. G. and Durkee, P. A. 1995 Ship-produced cloud lines of 13 July 1991. *Atmos. Environ.*, **28,** 3393–3403

Hobbs, P. V., Garrett, T. J., Ferek, R. J., Strader, S. R., Hegg, D. A., Frick, G. M., Hoppel, W. A., Gasparovic, R. F., Russell, L. M., Johnson, D. W., O'Dowd, C., Durkee, P. A., Nielsen, K. E. and Innis, G. 1998 Emissions from ships with respect to their effects on clouds. *J. Atmos. Sci.*, in press

Hudson, J. G. and Frisbie, P. R. 1991 Cloud condensation nuclei near marine stratus. *J. Geophys. Res.*, **96,** 20795–20808

Kilsby, C. G., Edwards, D. P., Saunders, R. W. and Foot, J. S. 1992 Water-vapour continuum absorption in the tropics: Aircraft measurements and model comparisons. *Q. J. R. Meteorol. Soc.*, **118,** 715–748

Lilly, D. K. 1968 Models of cloud-topped mixed layers under a strong inversion. *Q. J. R. Meteorol. Soc.*, **94,** 292–309

Martin, G. M., Johnson, D. W. and Spice, A. 1994 The measurement and parametrisation of the effective radius of warm stratocumulus clouds. *J. Atmos. Sci.*, **51,** 1823–1842

Nicholls, S. 1984 The dynamics of stratocumulus: Aircraft observations and comparisons with a mixed layer model. *Q. J. R. Meteorol. Soc.*, **110,** 783–820

1985 Aircraft observations of the Ekman layer during the Joint Air–Sea Interaction Experiment. *Q. J. R. Meteorol. Soc.*, **111,** 391–426

Radke, L. F., Coakley, J. A. and King, M. D. 1989 Direct and remote sensing observations of the effects of ships on clouds. *Science*, **246,** 1146–1149

Rawlins, F. and Foot, J. S. 1990 Remotely sensed measurements of stratocumulus properties during FIRE using the C-130 aircraft multichannel radiometer. *J. Atmos. Sci.*, **47,** 2488–2503

Rogers, D. P., Johnson, D. W. and Friehe, C. A. 1995 The stable internal boundary layer over a coastal sea. Part 1: Airborne measurements of the mean turbulence structure. *J. Atmos. Sci.*, **52,** 667–683

Saunders, R. W., Brogniez, G., Buriez, J. C., Meerkotter, R. and Wendling, P. 1992 A comparison of measured and modelled broad band fluxes from aircraft data during the ICE'89 field experiment. *J. Atmos. Oceanic Technol.*, **9,** 391–406

Shine, K. P., Fouquart, Y., Ramaswamy, V., Solomon, S. and Srinivasan, J. 1995 Radiative forcing of climate change. In *Climate change 1995.* IPCC report. Eds. J. T. Houghton, L. G. Meira Filho, B. A. Callander, N. Harris, A. Kattenburg, and K. Maskell. Cambridge University Press

Stevens, B., Cotton, W. R. and Feingold, G. 1998 A critique of one- and two-dimensional models of boundary layer clouds with binned representations of drop microphysics (12th International conference on clouds and precipitation, Zurich, Switzerland, 19–23 August 1996). *Atmos. Res.*, **47–48,** 529–553

Squires, P. and Twomey, S. 1960 The relation between cloud droplet spectra and the spectrum of cloud nuclei. In *Physics of precipitation. Am. Geophys. Union, Geophys. Monograph*, **5,** 211–219

Taylor, J. P. 1992 Sensitivity of remotely sensed effective radius of cloud droplets to changes in LOWTRAN version. *J. Atmos. Sci.*, **49,** 2564–2569

1993 'The remote retrieval of stratiform water cloud radiative and micro-physical properties'. Ph.D Thesis. University of Reading

Taylor, J. P., Edwards, J. M., Glew, M. D., Hignett, P. and Slingo, A. 1996 Studies with a flexible new radiation code. II: Comparisons with aircraft short-wave observations. *Q. J. R. Meteorol. Soc.*, **122,** 839–861

Twomey, S. 1974 Pollution and planetary albedo. *Atmos. Environ.*, **8,** 1251–1256